CEM 2016 – Mechanical Engineering Conference
Porto, Portugal, 1-3 June 2016
LAETA - Associated Laboratory for Energy, Transports and Aeronautics

DRONES SAFE FLIGHT: ON ADDRESSING OPERATIONAL SAFETY FOR LOW COST SMALL DRONES

Marta, A. C.[1]**; Moutinho, A.** [2]**; Gamboa, P.** [3]

[1] Center for Aeronautical and Space Science and Technology, IDMEC, Instituto Superior Técnico, Universidade de Lisboa, Portugal, andre.marta@tecnico.ulisboa.pt
[2] Center of Intelligent Systems, IDMEC, Instituto Superior Técnico, Universidade de Lisboa, Portugal, alexandra.moutinho@tecnico.ulisboa.pt
[3] Aeronautics and Astronautics Research Center, AeroG, Universidade da Beira Interior, Portugal, pgamboa@ubi.pt

KEYWORDS: *Unmanned Aerial Vehicle, Flight Energy Management, Mission Planning, Obstacle Detection and Avoidance.*

ABSTRACT: The recent exponential growth of small drones has been raising concerns about the safety of their operation. It is foreseen that embedded safety systems will become mandatory in the near future, when stricter operational regulations will be put in place. As such, the development of a low cost and low weight solution is paramount.
This work is part of the on-going research aimed to address the current lack of intrinsic safety systems by developing three distinct but highly coupled subsystems: the flight energy management (FEM), the mission planning (MP) and the obstacle detection and avoidance (ODA). Although aimed primarily to fixed wing drones, its conceptual design is general to any type of drones.
With the FEM, it is possible to estimate the energy balance of the current mission plan by making an assessment of the available energy, both stored and to be harvested in-flight (e.g., photovoltaic), and comparing it to the required energy, taking into account the aircraft performance and in-route weather conditions (e.g., wind and solar radiation). First principles of physics are used to obtain a baseline for the energy models without compromising future higher-fidelity models. The estimates can be done both pre-flight and continuously updated in-flight. This results in a real-time energy balance update that feeds the MP subsystem.
The MP allows for both pre-flight mission planning as well as adaptive in-flight mission planning, taking into account the data received from the FEM to attest its feasibility. It is based on a set of waypoints and a list of known fixed obstacles, such as terrain and buildings. The mission can be optimized for different metrics, such as time (minimum for fast execution or maximum for extended endurance), distance (maximum for extended range). This subsystem provides data to the drone operator that can be used to redefine the mission given the energy balance update. The MP feeds the FEM with the planned mission for the update of the required energy.
Lastly, the ODA comprises the hardware for sensing obstacles and the software for planning an evasive maneuver for collision avoidance. The detection of obstacles leads to an update of the list of known obstacles. Any maneuver triggered by the ODA is fed to the MP as it affects both the current mission and, consequently, the energy balance estimated by the FEM.
The goal is to develop a low cost safety system that can ensure the drone can either execute the mission successfully or it can prematurely return to the base safely.

1 DRONE MARKET OVERVIEW

According to the Teal Group [Teal,2014], drones, also known as Unmanned Aerial Vehicles (UAVs), are and will continue to be the sector in the world aerospace industry that exhibit the largest growth in the current decade. The spending is forecast to increase from $6.4 billion annually to $11.5 billion in the next ten years, totalling almost $91 billion in the next ten years. This tremendous growth will also see a shift of the cumulative civil market from 11% to 14% by the end of 2024.

While the development of drones emerged in the military industry as vehicles designed to perform dangerous missions, the proliferation of UAV technology and the cascading down effect, contributed decisively to the their application to civil missions. A report by NASA [Cox,2004] points the most common civil applications as border and costal patrol and monitoring, homeland security, law enforcement and disaster operations, digital mapping and planning, search and rescue, fire detection and firefighting management and power transmission line monitoring.

In recent years, the development of small low cost drones, made the hobbyist market the largest consumer of such vehicles, with sales forecasted by the Federal Aviation Administration to be in excess of one million units in the USA alone in Christmas 2015 [Karp,2015]. Among the top-three small UAVs manufacturers, that include Chinese DJI, French Parrot and US 3DRobotics, only very recently the former made available a somewhat limited obstacle sense and avoid system.

Being these low cost small drones at easy reach to the consumer, most often than not without any prior knowledge on how to operate such vehicles, there has been a very well founded concern about the safety of people and property in the vicinity of drones.

The goal of the current project is to develop low cost safety systems that can be easily embedded in current hobby UAV platforms. These systems are meant to assist the operator by providing information concerning the vehicle status in terms of capability to perform the mission and, ultimately automatically override the operator controls to avoid any catastrophic event.

The work focuses in three interconnected sub-systems: the flight energy management (FEM), the mission planning (MP) and the obstacle detection and avoidance (ODA). These sub-systems are tightly coupled to each other, as shown in Fig.1.

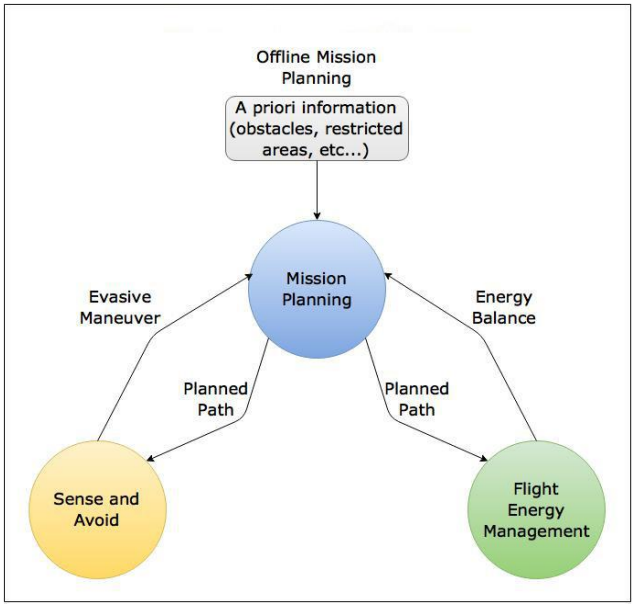

Figure 1. Control and video-subsystems [Baião,2016].

The interaction between the three subjects described above aims to enhance low-cost RPAS safety. Any flight should start with offline mission planning, accounting for known obstacles, restricted areas and any other relevant a priori information. Given the planned path, the obstacle detection module evaluates possible collision threats in real time, and if an evasive manoeuvre has to be performed, the mission planning module recalculates a possible flight path. Simultaneously, the energy management module evaluates the expected energy balance until the landing point, and if it is negative a new mission path has to be recalculated.

Notice however that, at these early stages of the project, each subsystem is being developed as an individual module, assuming the input data to be provided by the outputs of other modules is available.

2 UAV PLATFORMS

The work now being developed is built on a previous project of a Long Endurance Electric Unmanned Aircraft Vehicle (LEEUAV), that included the collaboration of research groups IDMEC at Instituto Superior Técnico and AEROG at Universidade da Beira Interior) [Marta,2014], both part of LAETA. The goal was to develop a low cost, small footprint electric UAV, capable of being deployed from short airfields, easy to build and maintain, and highly flexible to perform different civilian surveillance missions. The resulting design is illustrated in Fig. 2.

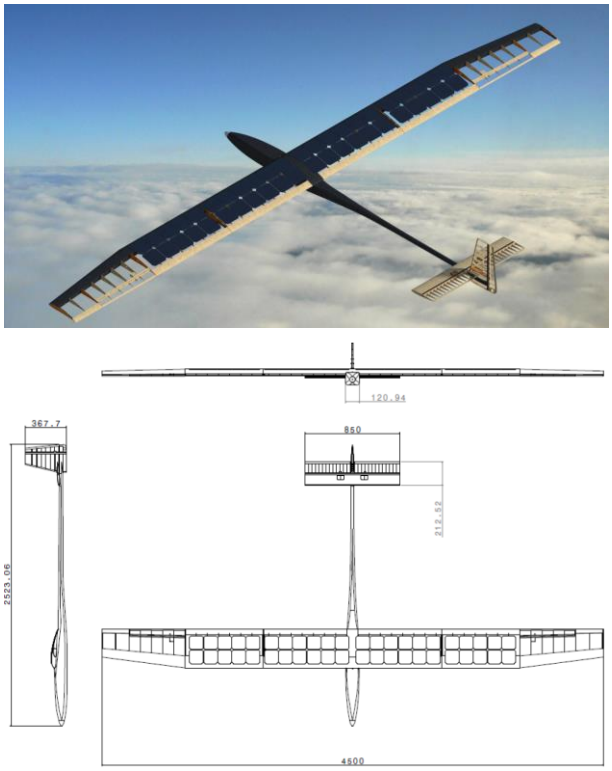

Figure 2. First generation LEEUAV [Marta,2014].

The LEEUAV mission comprises a 8-h long endurance daytime mission, at constant altitude (1000m above runaway) at a nominal cruise speed of 7.5m/s. The two main UAV specifications included: 1) long endurance, accomplished by using green power technologies such as an electric propulsion system with solar power, appropriate long endurance aerodynamic design and high strength to weight ratio structural design; 2) autonomous flight, accomplished by equipping the UAV with autopilot navigation systems. However, the obstacle avoidance capability was still missing.

Through this legacy project, some important lessons were learnt by addressing key design tasks: 1) several different electric propulsion system configurations were evaluated in terms of performance, overall weight and cost. It led to the selection of high-efficiency photovoltaic solar panels, high-density rechargeable batteries and combination of propeller with brushless electric motor [Ferreira.2014]; 2) using high-fidelity CFD analysis, the aerodynamic design of the airframe, including wing, fuselage and tail, was modelled. The computational process put in place enables the swift design of different UAV configurations [Silva,2014]; 3) the autopilot and Remote Person View (RPV) hardware and software were selected and tested in flight to assess its long range capability [Miller,2015]. The overview of the control and video sub-systems is shown in Fig. 3.

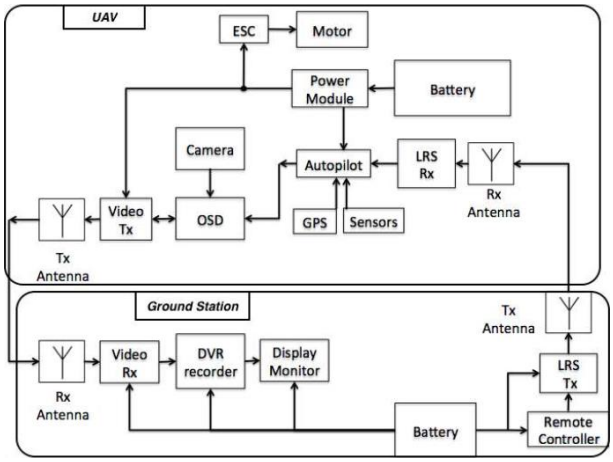

Figure 3. Control and video-subsystems [Miller,2015].

The prototype of first generation design

was built, using advanced model building techniques, and test flown radio control operated [Cândido,2014]. Although that prototype was far from being final, relevant conclusions arose from the tests performed concerning materials, manufacturing processes and flight quality.

Recently, a new generation fixed wing airframe started being developed [Parada,2016]. The selection of the new aircraft configuration was carried out using the Analytic Hierarchy Process (AHP) methodology [Saaty,1980]. The evaluation criteria were selected and weighted taking into account the importance of aircraft range,

$$R = E^{*} \eta_{total} \frac{1}{g} \frac{L}{D} \frac{m_{battery}}{m} \quad , \qquad (1)$$

where E^{*} is the battery mass specific energy, η_{total} is the electrical system total efficiency, L/D is the lift-to-drag ratio, $m_{battery}/m$ is the battery to total mass ratio. In addition, the hybrid propulsion system and the RPV nature of the aircraft were also taken into account. This led to a set of 10 weighted evaluation criteria: solar panel integration (20%), structures and weight (20%), aerodynamics (19%), propulsion (13%), RPV integration (11%), stability and control (4%), take-off and landing (4%), portability (4%), payload volume (3%), and manufacturing and maintenance (2%). This evaluation led to the V-tail configuration shown in Fig.4. The pusher design frees up the front of the aircraft for placing the RPV system.

Even though the described fixed wing platforms were the drivers for the current project, the safety systems to be developed are intended to be general in application, so that they can be embedded not only in fixed wing platforms but also rotary wing platforms (e.g. multicopters).

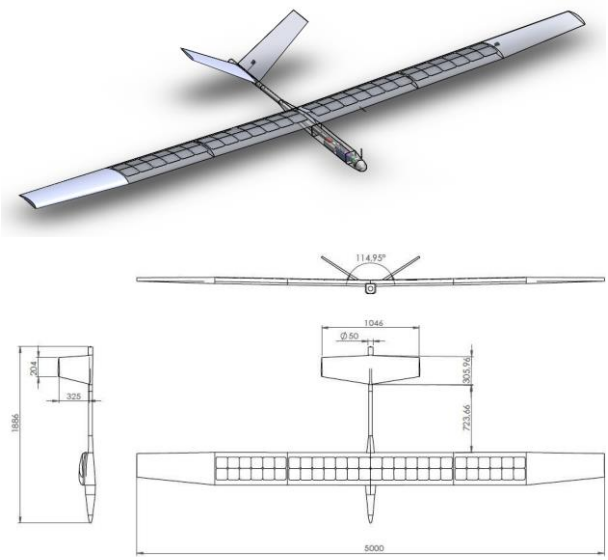

Figure 4. Second generation LEEUAV [Parada,2016].

3 FLIGHT ENERGY MANAGEMENT

The first safety module deals with flight energy management. Here the goal is to develop lower order mathematical models that estimate: 1) the available energy onboard from all sources; 2) the expected energy required to successfully complete the mission; 3) and interact with the mission planning module in real time, to ensure that the planned mission is adjusted given the weather conditions and unexpected obstacle avoidance, in such a way that enough energy is available to complete the mission safely or a return to base is forced if necessary.

The following tasks are expected to be accomplished:

- Model the energy available from all sources;
- Model the energy harvesting methods;
- Model the mission energy requirements;
- Identify the equipment necessary to perform the necessary parameter measurements;
- Calculate the energy balance for the mission;
- Perform case study simulations to assess the energy management module's performance;
- Integrate the final product in the LEEUAV's auto-pilot.

The diagram in Fig.5 represents the energy balance (remaining) at the end of the mission, at time t_f. The goal is to ensure that it is a positive balance, meaning the current aircraft mission can be completed.

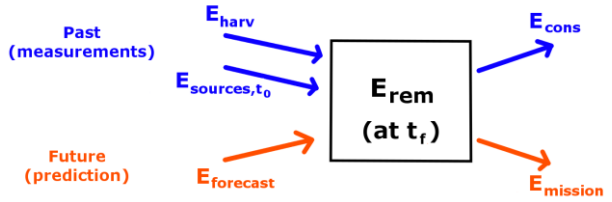

Figure 5. Energy flow in LEEUAV [Baião,2016].

Assuming that the assessment is being done at an arbitrary time t, ranging between the start t_0 and the end t_f of the mission, the energy remaining in the aircraft sources at the end of the flight can be written as

$$E_{rem,tf}(t) = E_{sources,t0} + E_{harv,t0\to t}(t) + E_{fore,t\to tf}(t) - E_{cons,t0\to t}(t) - E_{miss,t\to tf}(t), \quad (2)$$

where $E_{sources,t0}$ is the energy available in the energy sources before the flight (including the difference in mechanical energy due to difference in altitude of the departure and arrival airports), $E_{harv,t0\to t}(t)$ is the energy that was harvested through the solar panels from the start of the mission until a given instant, $E_{fore,t\to tf}(t)$ is the amount of solar energy expected to be harvested according to the weather forecast, $E_{cons,t0\to t}(t)$ is the energy that is estimated to have been consumed throughout the mission, from the start to the instant of calculation, and $E_{miss,t\to tf}(t)$ is the energy that is expected to be consumed from a given instant until the mission is complete. Notice that all quantities are a function of mission time, except for the energy available in the sources before the flight, since that is a constant amount.

3.1 Energy sources

Energy sources supply the energy the aircraft and its systems require to function properly. The main sources of energy found in most unmanned aerial vehicles are fossil fuels, batteries, and solar energy harvesting. For this project, fossil fuels are not considered.

The energy available in one source at a given time instant will be estimated with mathematical models, and the energy consumed since the start of the mission until a given instant can be obtained from

$$E_{cons\_source,t0\to t}(t) = E_{source,t0} - E_{source,t}(t), \quad (3)$$

and the energy consumed from all sources,

$$E_{cons,t0\to t}(t) = \sum_i E_{cons\_source\_i,t0\to t}(t) + E_{harv,t0\to t}(t), \quad (4)$$

where the energy harvested by the solar panels have been accounted for.

Fossil fuels

One of the reasons fossil fuels thrived in aeronautics is because of their very high specific energy content.

The mechanical energy extracted from the fuel chemical energy, by an engine of known efficiency, can estimated from

$$E_{fuel,t}(t) = u_{fuel} \times \rho_{fuel} \times V_{fuel,t}(t) \times \eta_{engine}, \quad (5)$$

where u_{fuel} is the fuel specific energy, ρ_{fuel} is the fuel density, $V_{fuel,t}$ is the volume of fuel and η_{engine} is the engine efficiency. Knowing the volume (or weight) of fuel at the start of the mission, and provided that the aircraft has a flow meter sensor, the available mechanical energy available at a given time t can be estimated from Eq.(5) using the estimated available volume of fuel,

$$V_{fuel,t}(t) = V_{fuel,0} - \sum_t \dot{V}_{fuel,t} \times t, \quad (6)$$

where $\dot{V}_{fuel,t}$ is the measured volumetric flow rate.

Batteries

Batteries are especially interesting because they can be recharged and reused many times. The most common types of rechargeable batteries are based on lead, nickel or lithium. While lead-acid (Pb), Nickel-Cadmium (NiCd) and Nickel metal hydride (NiMH) batteries are widely used for their low cost, their low specific energy content make them inappropriate for powering UAVs. Lithium-ion (Li-on), Lithium-ion polymer (LiPo) and Lithium-Sulphur (Li-S) are the best alternatives to power solar powered aircraft. These are the focus of battery research in the present for their very high specific energy, but some elements used in their composition make them even more expensive, and special care in operation must be taken because of the reactivity and flammability of Lithium. Table 1 summarizes the properties of the common battery types discussed.

Table 1. Battery properties [Gao,2015].

	Specific energy [Wh/kg]	Lifetime [cycles]
Pb	30	300
NiCd	50	1500
NiMH	75	1000
Li-Po	200	1000
Li-S	350	1000

The electrical energy consumed from a battery can be measured, at a given time instant, as

$$E_{cons\_bat,t}(t) = \sum_i P_i \times T_s = \sum_i V_{battery,i} \times I_{battery,i} \times T_s \quad (7)$$

where P_i is the instantaneous power measured at time instant i, and T_S is the sampling time of the measurement of battery current, and $V_{battery}$ is the battery voltage and $I_{battery}$ is the instantaneous current. This implies that both voltage and current sensors are to be installed in the battery circuit of the aircraft.

Knowing the energy stored at the start of the mission, $E_{battery,0,}$ either by using the manufacturer rated capacity or by measuring the energy fed by the charger, the available electrical energy available at a given time *t* can be estimated as

$$E_{battery,t}(t) = E_{battery,0} - E_{cons\_bat,i} - \sum_t R_{in} \times I_{battery,i} \times T_S \quad (8)$$

where R_{in} is the internal resistance. The last term in Eq.(8) corresponds to the energy dissipated by heat due to the Coulomb effect. The internal resistance value, even if provided by the manufacturer, should be experimentally measured according to the procedure in [Tremblay,2007].

Solar energy harvesting

Solar cells make use of the photoelectric effect to convert solar radiation into electric current, that can be used to power a load. A photovoltaic (PV) solar array is made of a set of solar cells arranged in serial and/or parallel, to provide the desired voltage and power.

Most solar cells are made of crystalline silicon, and they can be either monocrystalline or polycristalline. They have a long lifetime and are able to be mass produced easily. Amorphous silicon thin-film silicon solar cells are less expensive than the crystalline versions, but have lower efficiencies. Other newer chemistries such as crystalline Gallium arsenide (GaAs) offer the current best efficiencies but their cost is still prohibitive. The highest efficiencies offered for these chemistries are summarized in Tab.2.

Table 2. Photovoltaic cells comparison [NREL,2012].

	efficiency	cost
Monocrystalline Si	25%	high
Polycrystalline Si	21%	medium
Amorphous Si thin film	14%	low
Crystalline GaAs	44%	very high

The average power density reaching the Earth, just outside its atmosphere is 1366 W/m^2, but

at low altitudes (up to 2000m) where the UAVs are expected to operate, the maximum solar radiation does not exceed 1000 W/m^2.

Typically the solar panels are connected to batteries through a solar charger that has a Maximum Power Point Tracking (MPPT) capability. This ensures that the pair voltage-current provided by the panel is such that power is maximized. PV modules have a non-linear current-voltage (I-V) characteristic, and there is only one point at which it can provide maximum power. However, this point changes with solar radiation intensity and temperature, and if this is not accounted for, the mismatch in impedance between the PV modules and the load leads to power losses. The MPPT controller tracks the point of maximum power and adjusts the impedance of both the PV modules and the load, in order to have the maximum amount of power transferred to the load [Başoğlu,2016].

The energy harvested through the PV panels, from the start of the mission to a given time instant, can be expressed as

$$E_{harv,t0 \to t}(t) = \sum_i P_i \times T_s = \sum_i V_{solar,i} \times I_{solar,i} \times T_s \,, \quad (9)$$

where V_{solar} is the PV voltage and I_{solar} is the instantaneous current. This implies that both voltage and current sensors are to be installed between the solar MPPT charger and the battery.

To obtain the energy expected to be harvested from the solar panels from a given time instant until the end of the mission, it is necessary to estimate how temperature and irradiance will change over time. If these functions are known, then the energy that is expected to be extracted through the solar panels can be given by

$$E_{harv,t \to tf}(t) = \int_t^{tf} P_i dt = \sum_i \eta_{PV} P_{solar,i} T_s \,, \quad (10)$$

where η_{PV} is the efficiency of the PV panel, typically given by the manufacturer as a function of temperature, and P_{solar} is the solar irradiated power, that can be estimated as

$$P_{solar,t}(t) = R_{solar}(t) A_{PV} \,, \quad (11)$$

where R_{solar} is the solar irradiance and A_{PV} is the PV surface area. Consequently, it is necessary to either measure the irradiance by using a pyranometer or to access databases of historical data for a particular location.

Mechanical energy

Another type of energy that should be considered as a source of energy is the mechanical energy of the aircraft. This is simply modelled as the sum of kinetic E_k and gravitational potential energy E_p,

$$E_{mechanical,t}(t) = E_{k,t}(t) + E_{k,t}(t) = \\ = \frac{1}{2} m v(t)^2 + mgh(t) \,, \quad (12)$$

where m, v and h are the aircraft mass, speed and altitude, respectively, and g is the gravitic acceleration. To calculate this energy, the aircraft current speed and altitude needs to measured, using for instance a Pitot tube.

If there is a change in either speed of altitude, then the variation of mechanical energy has to be due to the work made by the forces actuating on the aircraft (except its weight that is accounted by the gravitational potential energy).

3.2 Energy consumption

Any aircraft will consume a given amount of energy to take-off, climb, descent, manoeuvre, accelerate, gather and process data. The specifications for the vehicle's components and its dynamic, along with the energy requirements imposed for any aircraft, will dictate how much energy has to be extracted from the energy sources to execute a given command.

In general, the propulsion system is the main energy sink in an aircraft, but other lower powered components will contribute to the energy expenses, namely other actuators (to accomplish varied manoeuvres), sensing and communication equipment (to transfer data) and processing units (that will process that

data).

3.3 Energy required

The mathematical model for the estimation of the energy required to complete a planned mission, is based on

$$E_{mission,t \to tf}(t) = W_{prop,t \to tf}(t) + E_{av,t \to tf}(t), \quad (13)$$

where W_{prop} is the energy required by the propulsion system and E_{av} is the energy required by the avionics equipment and other auxiliary systems onboard, both from a given instant until the end of the planned mission.

From the principle of work and energy, the change in kinetic energy of a body is related to the work done by the external forces acting on it,

$$E_{k,t}(t) = W_{ext\_forces,t \to tf}(t) + E_{k,tf}(t), \quad (14)$$

If the work done by the weight is accounted as a change in gravitational potential energy.

The work required to be done by the propulsion system, for the aircraft to accomplish its mission, can be estimated using

$$W_{prop,t \to tf}(t) = W_{drag,t \to tf}(t) + E_{k,t \to tf}(t) + E_{p,t \to tf}(t), \quad (15)$$

being the work done by drag,

$$W_{drag,t \to tf}(t) = \int \vec{D} \bullet d\vec{s}, \quad (16)$$

where D is the drag force and s is the displacement vector. The energy dissipated by the drag W_{drag}, accounted for in the calculation for the required energy, will vary with the path chosen for the mission, as well as the aircraft's aerodynamics and velocity over time.

Note that the kinetic E_k and potential E_p energies are accumulated quantities, meaning that they are only accounted for when energy from the sources is exchanged for a change in speed or altitude. For instance, when the aircraft loses altitude, the loss in potential energy can be converted into a gain of kinetic energy or to compensate the energy dissipated by drag, thus reducing the required work of the propulsion system. This becomes clear by recognising that the change in mechanical energy can be written as

$$E_{k,t \to tf}(t) + E_{p,t \to tf}(t) = E_{k,tf}(t) - E_{k,t}(t) + E_{p,tf}(t) - E_{p,t}(t). \quad (17)$$

The energy required to operate all avionic systems (sensors, communications, low power actuators and processors), from a given time until the end of the mission, is given by the sum

$$E_{av,t \to tf}(t) = E_{sens,t \to tf}(t) + E_{comm,t \to tf}(t) + E_{lpa,t \to tf}(t) + E_{proc,t \to tf}(t). \quad (18)$$

To estimate these quantities, it is necessary to quantify the rated power consumption of each electric/electronic component and their operating scheduling during the mission.

A schematic of the contributions to the predicted energy required to complete the mission is shown in Fig.6.

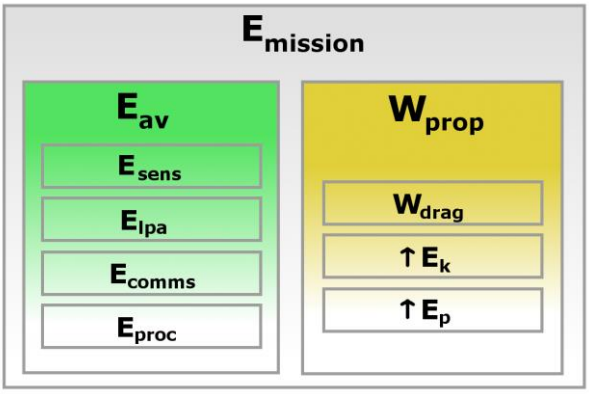

Figure 6. Estimated required energy [Baiao,2016].

3.4 Energy management

Energy management methods aim to make the most efficient use of available energy. In aircraft that only possess one type of energy source, the energy management is straightforward, all the energy required to fly and operate the vehicle will come from that source. However, some UAVs, such as the fixed-wing platform adopted in this project, have a hybrid setup installed, with more than

one source of energy.

The most common hybrid system is the electric propulsion vehicle that carries a rechargeable battery and recharges them using PV cells. Energy harvested through the PV cells can be directly used to power the aircraft, when enough energy is being collected, and when this is not the case, some energy can be extracted from the battery to provide the remaining energy required for operation. If PV cells harvest more energy than the one they need to power the aircraft, then the battery can be recharged with the excess power. To prevent overcharging and to increase battery life, many solar powered aircraft incorporate a charge controller (or charge regulator) connected to their batteries, which manages the current flow to and from them, and may even protect them against overvoltage.

To optimize the usage of energy to maximize the endurance of a UAV, an appropriate energy management system (EMS) has to be developed. A possible approach, described by [Gao,2013], suggests a three stage flight. Stage one begins when enough solar energy is available to be harvested by the PV panels to power the aircraft, and the excess energy is used to charge the batteries. Moreover, during stage one, the aircraft gains as much altitude as possible, storing energy as gravitational potential energy. During stage two, when the solar power available is not enough to maintain level flight (e.g., at dusk or night), the aircraft trades the accumulated potential energy for kinetic energy, remaining in gliding flight and losing altitude. Finally, stage three starts when the aircraft descended into the lowest operational altitude, and at this point the batteries supply the energy required to maintain level flight. This strategy taken to to limit can allow for multiple day non-stop flights.

When a combination of fossil fuels and rechargeable batteries, or fuel cells (FC) and rechargeable batteries are used, it would be wise to first drain the energy from the batteries and avoid as much as possible to resort to the use of the non-rechargeable energy sources, since the energy consumed from the batteries could be recovered by means of solar energy harvesting through the PV cells. However the specific energy of batteries is usually smaller than that of the other energy sources. Because of their weight, batteries end up being a secondary onboard power source in most cases. [Karunarathne,2012] studied an EMS with a fuel cell and battery combination. Three modes of operation are described: during start-up, the battery powers the propulsion system while the FC system gradually starts its operation and providing power to the load; once the FC is fully operational, the battery is recharged to at least 90\% of its capacity before take-off; during the most power demanding conditions (take-off, climb and maximum velocity) both the battery and the FC power the propulsion system, but when the aircraft is in cruise, only the FC supplies power to it, while also recharging the battery.

The EMS should not only manage the energy required but also take into account the rate at which it is used, that is to say, the power required. If the total drag curve is known for every airspeed, the power required curve can be obtained by

$$P_{req} = D \times V = \frac{1}{2} \times \rho \times V^3 \times S \times C_D , \qquad (19)$$

where ρ is the air density, V is the true airspeed, S is the reference wing area, and C_D is the total drag coefficient.

The black curve in Fig.7 represents a typical required power curve to fly at a given airspeed, for a propeller aircraft and assuming a constant high-lift device configuration. The minimum controllable airspeed is the stall speed (where the black curve becomes continuous). The airspeed at which the power required is minimum does not correspond to the airspeed to fly with minimum drag, the second one occurs at a slightly higher airspeed, approximately at the best rate of climb speed point. At airspeeds below or above the minimum power required one, the power required increases due to an increase in induced drag (since the aircraft has to fly at an

higher angle of attack to remain in flight) and due to an increase in parasitic drag respectively.

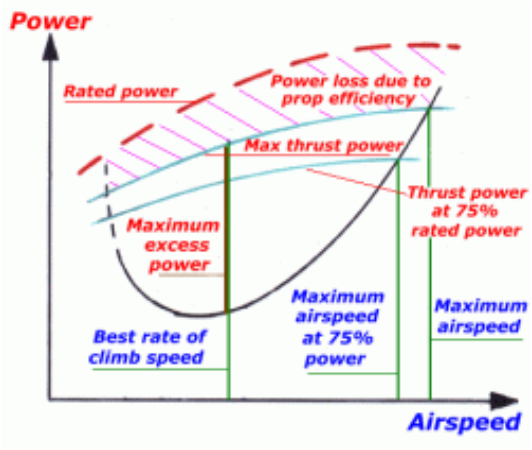

Figure 7. Required and available power. [Baião,2016].

The red dashed curve represents the rated engine power (full throttle engine power delivered to the propellers in levelled sea-level flight), but the first blue line represents the maximum thrust power available after accounting for the propeller efficiency. The airspeed at which the first blue curve and the power required curve intersect indicates the maximum attainable airspeed. Moreover, the region between the maximum thrust power curve and the power required curve, for a given airspeed, illustrate the excess power available to perform manoeuvres. The airspeed at which this excess power is maximum is an ideal candidate (maximum rate of climb) for the rate of climb speed. The second blue curve indicates the available power at 75% rated power, and a similar analysis follows from the previous curve. It is important to note however that the maximum power available varies with altitude (due to decreased air density with altitude), and when full throttle is applied at altitudes above sea-level, the maximum power available will drop to a percentage of the rated power. At an altitude where full throttle nets only 75% of the rated power, the corresponding airspeed obtained corresponds to the point of intersection of the second blue curve with the required power curve.

Knowing the mission profile and the desired flying speed at each mission segment, it is then possible to estimate the power required to fly the aircraft. Each of the energy sources identified previously (fossil fuel engine or battery/FC/PV fed electric motor) have a maximum available power, that have to be match to the required power. This is the main driver for the EMS to determine the appropriate source of energy to by used at a given time, as illustrated in Fig.8..

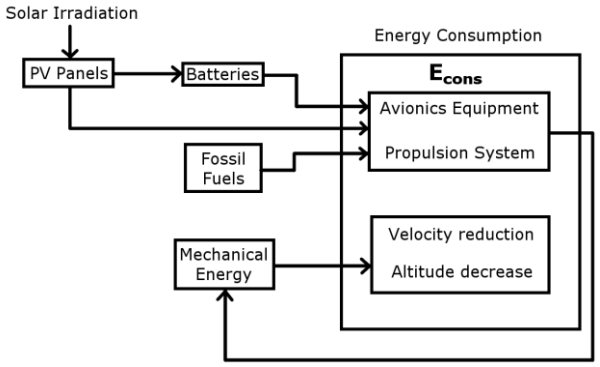

Figure 8. Energy and power management system [Baião,2016].

Given the hybrid solar and battery powered LEEUAV platform, a solar energy management algorithm was developed in MATLAB®, illustrated in Fig.9. Given the available battery energy and power, the PV array and MPPT solar charger controller properties, the irradiation forecast for a specific location, and the mission profile, this algorithm determines the minimum available PV area required to fulfil the endurance target.

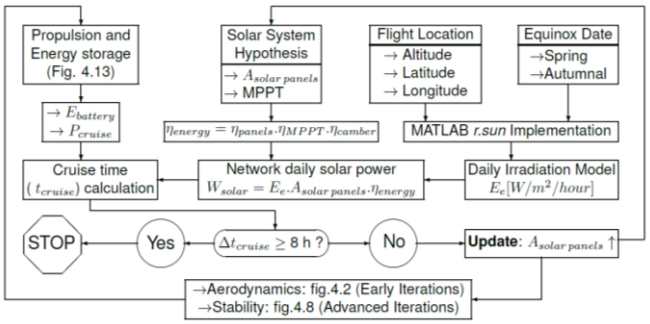

Figure 9. Hybrid solar-battery design [Parada,2016].

4 OBSTACLE DETECTION AND AVOIDANCE

Sense and Avoid (S&A) technology is fundamental to ensure a safe integration of unmanned aircraft in a congested airspace and increase their autonomy, and will probably propel the creation of regulations regarding UAVs in the future. The general structure of an S&A system is depicted in Fig.10.

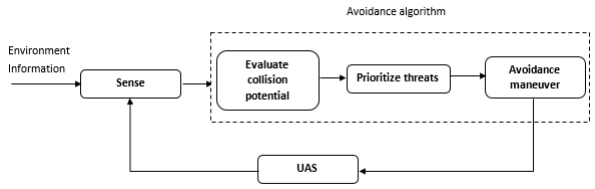

Figure 10. Functionalities of S&A system [Alves,2016].

Requirements and standards for S&A systems are still under development, but the system will be expected to provide two main functions: maintain a minimum self-separation and perform, or suggest, manoeuvres to avoid collisions when all safety layers fail. Among these functions, the S&A sytem is expected to provide a set of sub-functions [ICAO,2014]: 1) Detect, determine presence of aircraft or other potential hazards; 2) Track, estimate position and velocity (state) of a single intruder based on one or more surveillance reports; 3) Evaluate, assess collision risk based on intruder and UAV states; 4) Prioritize, determine which intruder tracks have met a collision risk threshold; 5) Declare, decide that action is needed; 6) Determine, decide on what action is required; 7) Command, communicate determined action; and 8) Execute, respond to the commanded action.

4.1 Sense and avoid framework

S&A systems consist of sensing hardware, a decision mechanism, a path planner and a flight controller.

The sensing equipment collects information about other traffic and obstacles. It can be classified as cooperative when any two aircraft have the same sensing equipment on-board and are able to exchange information through a communication channel, for example using a transponder (similar to Traffic Collision Avoidance System (TCAS)). However, small UAVs have strict payload capacities and this factor has to be accounted for. Automatic Dependent Surveillance - Broadcast (ADS-B) is a recent technology that broadcasts the aircraft's position, velocity and its intent, using GPS data, it is lighter than TCAS and is considered to be the future of surveillance technology. However, even if every aircraft was equipped with cooperative sensing systems, it would still be impossible to detect other obstacles like buildings and mountains. Aircraft not equipped with such devices rely on non-cooperative sensing to detect traffic or static obstacles [Yu,2015]. Among the non-cooperative technologies the sensing principle can be active or passive. Active sensors, such as radars and laser (e.g. Synthetic Aperture Radar (SAR), Light Detection and Ranging (LIDAR)), emit a signal that is reflected by the obstacle allowing its detection. Passive sensors depend on the reception of signals emitted by the obstacle itself, they include electro-optical, infra-red and acoustic technologies.

The decision mechanism (software algorithms) then analyses the data collected through the sensing hardware and verifies if the current planned trajectory has to be altered to avoid threats, and if that is the case the path planner will attempt to generate an alternative path given the constraints on vehicle dynamics and fuel economy, which should be optimal when possible. Finally, the flight controller outputs the control signals that will allow the aircraft to perform an evasive manoeuvre. S&A is a time critical system that will not have the ability to prevent collisions if the computation time for all the mentioned tasks exceeds a given threshold [Yu,2015].

The proposed collision avoidance system framework is expected to account for both static and dynamic obstacles and follows a two layered architecture, as illustrated in Fig.11. In the first stage, the global planning module,

which assumes a known static environment, determines a collision free path from a given start to goal configurations. The RPAS then follows this path and as new threats are detected by the on-board sensors, the local planning module must re-plan the path while avoiding these new obstacles. The two stage planning architecture allows the offline and online solutions to compensate each other in terms of planning horizon, considered obstacles, vehicle and mission constraints.

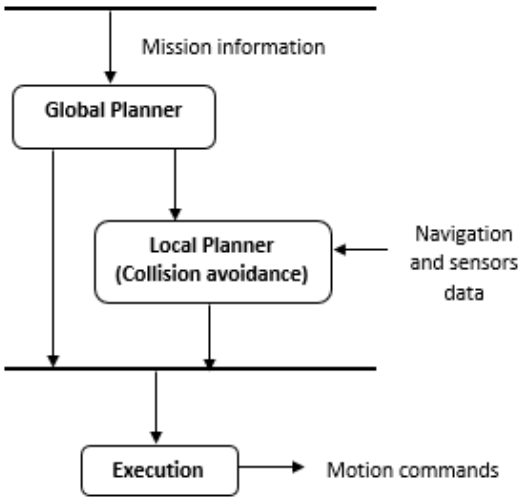

Figure 11. Proposed collision avoidance framework [Alves,2016].

In this work, the type of sensors used will not be specified, but it is assumed that there is a working method of sensor fusion to obtain the necessary information about the environment. To develop the collision avoidance algorithms, this information will be provided in tabular form as shown in Tab.3.

Table 3. Obstacle database structure [Alves,2016].

Obstacle #	X, Y, Z	R, H, D
1	x_1,y_1,z_1	r_1,h_1,d_1
2	x_2,y_2,z_2	r_2,h_2,d_2
…	…	…

Each known obstacle base location is defined by its coordinates *(x,y,z)*. For the purpose of collision avoidance, a safety volume is defined. Due to its simplicity and ability to encompass a wide variety of obstacle types a cylindrical model is used to represent obstacles, being *h* and *d*, the cylinder height and radius. From these values, and knowing the RPAS position from the navigation module, the distance *r* to the obstacle is determined. This distance will be used to rank the table in order to prioritize closest obstacles. This ranking is not necessary for the offline planning stage but it will be important during real-time implementation.

For moving obstacles detected during the mission execution, the same information is to be provided, with the additional intruder velocity also included. For this type of threats, the relative distance is not enough to evaluate the urgency with which the threat must be addressed hence the time to collision will also have to be considered.

The global planner depicted in Fig.10 is a module that receives a set of waypoints during the mission planning stage, a known obstacle data-base and a terrain map. If obstacles are found in the segments that connect the given waypoints, a free path, that satisfies certain optimization criteria such as shortest path, is provided in the form of a waypoint matrix, as schematized in Fig.12.

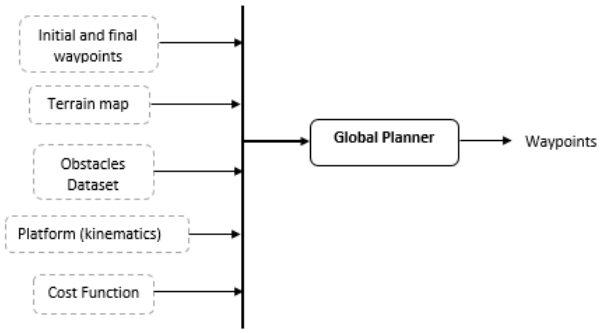

Figure 12. Global planner inputs and outputs [Alves,2016].

Given a set of (adjusted) waypoints, the RPAS is then guided to the desired locations using either path following or path tacking techniques. The objective of path following is to minimize the position error, forcing the control output to follow a path with no time dependence. Path tracking requires the vehicle to follow a time and space reference trajectory, not being as flexible as the path following

approach.

When unexpected obstacles appear, the local planner is activated to generate a new path. The online collision avoidance will perform two main tasks: the detection of possible collisions and the provision of avoidance manoeuvres. The local planning module will receive from the navigation module the current RPAS position and velocity, information from the sensing module and the list of waypoints of the pre-planned path. When new obstacles are detected in the sense table, the collision detection algorithm is activated to determine if there is a collision risk. If a collision is eminent, an appropriate evasive manoeuvres, which might be defined by new waypoints or velocity and heading commands, is determined by the collision avoidance algorithm. Efficient obstacle avoidance should respond quickly to unexpected obstacles and be optimal in respect to the overall mission goal and vehicle dynamics.

4.2 Collision avoidance algorithms

Among the several existing collision avoidance algorithms, three stand out as being the most common.

The Artificial Potential Field (APF) [Luo,2014] method is inspired by physical potential fields and is generally used for reactive collision avoidance systems [Ruchti,2014]. The aircraft is treated as a charged particle moving through a field induced by attractive and repulsive forces. Waypoints to visit are modelled as attractive forces that direct the UAV towards the goal. In contrast, detected obstacles are modelled as repulsive forces, whose magnitude depends on the distance between UAV and obstacles. The control command is then given by the sum of the attractive and repulsive forces. When compared to other methods, the APF method is popular due to its mathematical simplicity which is an advantage in terms of computation speed and complexity [Lihua,2016], making it appropriate for use in real time.

The Geometric Solution (GS) is another method of addressing the collision avoidance problem. This method attempts to use simple geometric relations to obtain a collision avoidance solution. A representative example is the collision cone formulation. This approach uses RPAS position, heading and velocity to determine if the propagated trajectory will result in the violation of a minimum separation distance. The idea is to keep the RPAS velocity vector out of the region surrounding the intruder. In [Luongo,2009], a 3D solution is presented for non-cooperative collision avoidance of aircrafts, where algorithm combines velocity, heading and vertical changes to avoid the safety volume around the intruder aircraft.

The Markov Decision Process (MDP) approach formulates the collision avoidance problem as an optimal control of a stochastic system. A MDP is a discrete dynamic programing process where the state of the system changes according to the current state and the chosen action. The problem is then solved through dynamic programing by evaluating the expected reward for each combination of states and actions. A variant called Partially Observable MDP (POMDP) was devised to account for uncertainties that may arise from sensors and intruder behaviour. The MDP approach accounts for all possible encounter scenarios and their likelihood when solving the model, allowing the automatic generation of the collision avoidance logic by defining the system goal and operating environment. For a collision avoidance system the state must contain at least the 3D positions and velocities of at least two aircrafts and in order to build an optimal policy and all the possible combinations of actions-state must be considered. Large state spaces are the main issue when solving MDPs as some formulations would require too much computational complexity to solve the problem, making the approach restricted to offline planning. Examples of POMDPs applied to RPAS collision avoidance can be found in [Temizer,2010] using a 2D formulation assuming a discrete state space

and [Bai,2011] extending it to 3D continuous-state models.

5 MISSION PLANNING

Mission planning, or path planning, attempts to find the optimal collision-free path for the UAV to complete the mission, given several constraints and known environmental conditions. The optimization can aim to minimize the distance, the energy required or the mission time, or maximize the endurance of the aircraft.

In general, path planning requires the collection of external information, namely the number, position and velocity of obstacles, as well as pre-flight information, like the goal position, terrain and restricted areas. This information is processed afterwards and, faced with the set of requirements for the mission, the vehicle's dynamics and navigation parameters, a path is generated by the system. Since it is likely that the aircraft will face unexpected obstacles, including other traffic, the initial planned path will need to be corrected in certain sections, until the goal position is reached.

5.1 Global and local path planning

Global path planning algorithms, which are mainly performed offline, generate a low resolution path that reaches the goal point while local planning gives a high resolution path over a segment of the global path avoiding small obstacles. These local algorithms are usually fast and reactive, performed online to ensure the vehicle safety from unexpected obstacles (such as moving aircrafts or objects too small to be present in the data base).

5.2 Path planning algorithms

Several approaches exist for determining paths given some representation of the environment. The most popular techniques are described next.

5.2.1 Graph search

Graph search algorithms are one of the most popular methods used in robot path planning. In these algorithms, the airspace is discretized and represented by a set of cells on a weighted graph. The robot's configuration is represented by the graph nodes while the edges connecting the graph represent the cost of moving between nodes. High weight values on cell edges can be used to represent obstacles. Most of the graph search algorithms are based on the Dijkstra algorithm [Dijkstra,1959]. This algorithm works by evaluating the cost of moving from one node to its neighbours and connecting the nodes with the lowest moving cost. The A* algorithm [Duchon,2014] builds on the latter by combining the moving cost between nodes and the cost to reach the goal to drive the search. The problem with these algorithms, due to its graph structure, is that they usually calculate paths with unnecessary heading changes. Generally post-processing techniques must be applied to obtain a flyable path. They also only apply to known static environments, which imposes a limit for agents in uncertain environments. To overcome this limitations D* and T* were introduced. Dynamic A* improves on the A* algorithm making it applicable to dynamic environments by allowing the edges cost to be dynamically adjusted [Liao,2012]. T* [Daniel,2010] is meant to deal with the problems of heading constraints in a graph structure by considering different connections between graph nodes. Paths obtained by T* are smoother than those determined by A*. Both algorithms were successfully applied to the UAV path planning problem in [Filippis,2012]. A major downfall when applying typical graph search algorithms to path planning problems is lack of inclusion of the vehicle kinematics. In [Hwangbo,2007] node connection rules are defined to include the vehicle kinematics. A small fixed wing UAV is considered, and the grid size in the

horizontal place (x and y directions) is defined by the minimum turning radius, while the size in vertical axis (z direction) is defined by the maximum climb angle (assuming constant speed). The graph search algorithms are attractive because they are easy to implement and can be adapted to different case scenarios by allowing distinct heuristics to guide the search.

5.2.2 Rapidly exploring random tree

Rapidly Exploring Random Tree (RRT) [Kothari,2013] is a popular search algorithm when dealing with high dimensional spaces. The general idea is to connect points sampled randomly from the search space. The algorithm is initialized with a graph that contains only the initial state as a single vertex. At each step, a random sample from the search space is generated and an attempt is made to connect this new sample to the nearest vertex on the tree. This connection is limited by a growth factor (generally distance), if the connection is successful then the new sampled point is added to the graph. By increasing the probability of sampling states in a specific area, the search is guided toward the goal state. The higher this probability is, the greedier the algorithm. In [Lin,2015] a greedy version of closed-loop RRT is used to plan the collision avoidance path.

5.2.3 Ant colony optimization

The Ant Colony Optimization (ACO) algorithm is a meta-heuristic approach inspired by the foraging behaviour of ants in the real world. Ants are known to find the shortest path from their nest to the food source. They accomplish this by leaving a pheromone trail along their path. This trail is detected by other ants which will tend to follow the trail with higher pheromone levels. The ACO formulation has also been applied to the UAV path planning problem [Ma,2007]. These solutions however are only applied to 2D environments, considering a constant flying height, which is not suitable for many applications of flying vehicles. ACO has shown good results in planning paths but the computation time is prohibitive for online applications.

5.2.4 Mixed integer linear programming

Mixed Integer Linear Programming (MILP) [Grøtli,2012] is a technique that addresses the collision avoidance problem using linear programing. To solve the MILP problem a set of constraints to model the UAV dynamics must be specified, additionally constraints related to collision avoidance, such as separation distance, must be provided. Once the problem is formulated, a solver determines the solution. This approach however is computationally expensive and only feasible for offline planning as it scales poorly with the problem size. This formulation has been widely applied to the collision avoidance problem of UAVs [Richards,2012].

5.3 Path planning process

For the path planning process, it is assume that the following elements are available:

- Ordered set of goal waypoints;
- Environment (terrain, static obstacles and wind conditions);
- Cost function of mission objective.

Based on these, the path planning algorithm produces a safe flyable path for the RPAS. The planned route consists of a set of waypoints in the form

$$P = \left\{P_1 \ldots P_n\right\} \quad , \qquad P_i = \left(x_i, y_i, z_i\right). \quad (20)$$

The planned trajectory should account for speed and manoeuvre constraints of the vehicle. The path planning process is divided in four steps:

1. Representation of the configuration space, or planning environment;
2. Definition of constraints (both vehicle and mission related);

3. Definition of the cost function;
4. Search process for the optimal path from starting point to target point.

These will be covered in the next sub-sections.

5.3.1 Environment modelling

A key concept of path planning is the representation of the physical world where the RPAS will operate. The environment model includes terrain, weather and obstacles.

The configuration space is a data structure that allows the specification of the possible UAV positions (location and orientation) and obstacles location. Many representations of configuration spaces can be used, the main ones being Voronoi diagrams, regular grids and quadtrees. For this project, regular grids are used due to their conceptually simple representation.

By properly defining the grid resolution, it becomes easy to find kinematically feasible paths. When deciding on the grid size some limitations of the RPAS must be considered. In the horizontal plane (*x*-*y*), the grid resolution is limited by the minimum turning radius of the RPAS, this is a restriction in the lateral acceleration of the vehicle. By setting the grid size to be at least 1.5 times greater than the minimum turning radius, the feasibility of the path is guaranteed, resulting

$$\Delta x = \Delta y = 1.5R_{\min} \quad . \tag{21}$$

Fixed-wing platforms are not allowed to climb at an angle superior to the maximum climb angle, γ_{max}, resulting in a limitation in the resolution along the vertical plane *z*,

$$\Delta z = \Delta x.\gamma_{\min} \quad . \tag{22}$$

5.3.2 Platform constraints

Some of the kinematic constraints of the vehicle, minimum turning radius and maximum climb angle, were already included in the definition of the search space. Other constraints in the vehicle manoeuvrability can be included in the process of node expansion during the search process through the graph.

In a regular 3D grid, there are 26 neighbouring nodes per node. For a non-holonomic vehicle, such as multirotor, any of the points can be achieved from the central location but fixed-wing platforms have a forward only motion and cannot make sharp turns or climbs. These manoeuvrability restrictions are incorporated by defining a set of expansion rules [Hwangbo,2007]. Besides the RPAS position, given as (x,y,z), its heading and climb angle must also be included in the node definition in order to determine which manoeuvres are possible from the given configuration, as illustrated in Fig.13.

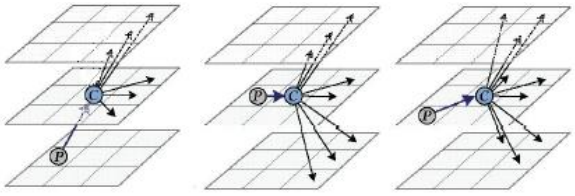

Figure 13. Expansion rules for fixed-wing platforms (adapted from [Hangbo,2007]).

5.3.3 Cost function

Depending on the mission objectives different cost functions can be considered. RPAS have limited range and endurance so in this project two different criteria are considered: minimum distance and minimum energy.

Minimum Distance

For the minimum distance paths, the cost function is simply given by the Euclidean distance between points. In the case the RPAS is moving between *i* and point *j* yields

$$d_{ij} = \sqrt{\left(x_i - x_j\right)^2 + \left(y_i - y_j\right)^2 + \left(z_i - z_j\right)^2} \quad . \tag{23}$$

Minimum Energy

The RPAS motion can be analysed using the

principle of work and energy.

Following Eq.(15) in Section 3.3, the required energy corresponds to the work done by the thrust generated by the propulsion system and additional avionics energy consumption. Considering the forces acting on the RPAS, the energy required to fly between points *i* and *j* can be expressed as

$$E_{ij} = \frac{1}{2} m\left(v_j^2 - v_i^2 \right) + mg\left(z_j - z_i \right) + D\Delta s_{ij}, \qquad (24)$$

where the terms in the rhs account for the variation in kinetic energy, the variation in gravitational potential energy and the energy dissipated by drag, respectively.

Wind has to be accounted in Eq.(24), where v corresponds to the air speed, which relates to ground speed as

$$\vec{v}_{ground} = \vec{v}_{air} + \vec{v}_{wind} \qquad (25)$$

The air displacement is given by

$$\Delta s_{ij} = v_{air} \Delta t_{ij} . \qquad (26)$$

where Δt_{ij} is the time required to fly from point *i* to *j*. To ensure that the RPAS follows the desired ground track, the component of $\vec{v}_{ground}$ transversal to the ground path must be zero.

5.3.4 Path search

The A* algorithm is regarded as one of the most practical an efficient path planning algorithm and, as seen in Sec.5.3.2, it can handle some vehicle kinematic constraints. As such, this method was the first approach in this project. The A* algorithm improves on classic graph search methods by combining aspects of both uniform cost search and greedy best first search. The nodes are evaluated according to the cost function

$$f(n) = g(n) + h(n), \qquad (27)$$

where *g(n)* denotes the cost to reach the node and *h(n)* represents the cost of getting from the node to the goal. As such, *f(n)* represents the estimated cost of the cheapest solution going through *n*.

Because the number of nodes to explore increases exponentially with the dimension of the graph, A* takes too long to find a feasible solution for more complex problems. In this case, an approximate solution that can be found faster may be more useful. To improve the algorithms performance there's an approach called Weighted A*. The WA* version makes use of a weighted sum of cost and heuristic to speed up the search process by reducing the number of explored nodes.

$$f(n) = g(n) + w.h(n), \qquad (28)$$

For $w>1$, there is a bias towards states that are closer to the goal. This weighted function improves the algorithms performance but optimality is no longer guaranteed as the heuristic is no longer admissible. The cost of the solution found is in the worst case *w* times greater than the optimal solution.

In order to evaluate the influence of *w* on the quality of the obtained solution, a test was run over a large search space. The search space characteristics for this test are given in Tab.4, and the terrain can be seen in Fig.13.

Table 4. Map characteristics [Alves,2016].

Map size	Start	Goal	$\Delta x = \Delta y$	Δz	D_{safety}
463x350x60	[51,439,200]	[324,258,200]	30	10	100

The values Δx and Δy correspond to a fixed-wing platform with minimum turning radius of *20m,* and the vertical spacing Δz corresponds to a maximum climb angle of approximately 18^o. A minimum safety distance of *100m* from any obstacles or terrain is defined. In this test, the cost function for the search was the distance travelled from the start state to the current state and the heuristic used was the straight line Euclidean distance from the current node to the goal. The average results for 30 simulations are presented in Tab.5.

All examples are obtained with MATLAB R2012b running on a Intel Core i7 with a CPU of 2.40 GHz, 8Gb RAM and Windows 8.1.

Table 5. Path search for fixed wing platform using A* e WA* algorithms [Alves,2016].

Weight *w*	# Eval. nodes	UAV Distance [m]	CPU time [s}
1	769422	1.0446e4	9621
1.1	1872	1.0460e4	0.4036
1.2	1871	1.0460e4	0.3993
1.5	1871	1.0460e4	0.3836
2	1868	1.0460e4	0.3885
5	1469	1.0512e4	0.3457
10	1439	1.0517e4	0.3175
25	1432	1.0539e4	0.3160
50	1429	1.0539e4	0.3160

The optimal and sub-optimal paths found can be seen in Figures 14 and 15.

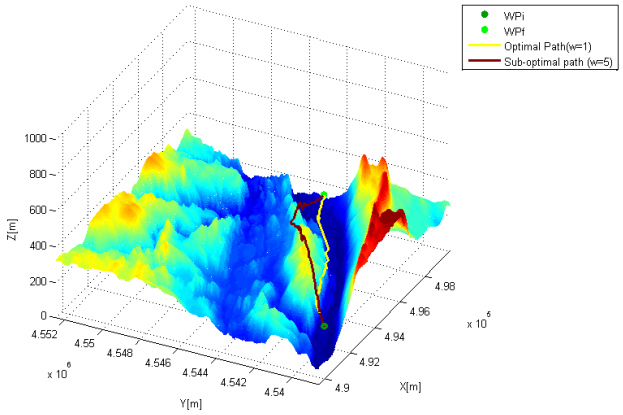

Figure 14. A* paths (3D views) [Alves,2016]).

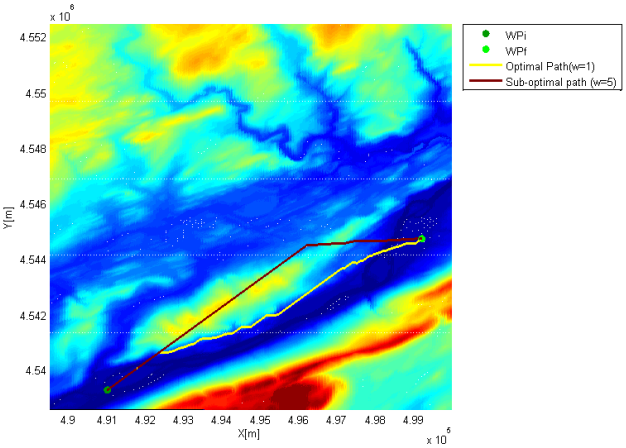

Figure 15. A* paths (*x*-*y* plane) [Alves,2016]).

From the obtained results in Tab.5, it can be seen that WA* provides a considerably faster execution time. Even the smallest increase in the weight over unity greatly reduces the number of explored nodes, biasing the search towards the goal. In this case, even for high weight values, the path cost is not much worse than the optimal (for *w=50*, the cost is only *1.3%* higher than the optimal). However, even though the increase in distance is not much higher, the path becomes less "flyable", as it includes numerous height changes along the path. During the offline computation stage, execution time is not an issue, but for the online implementation, the processing speed is key. In those cases, a compromise between path optimality and processing requirements may be necessary.

Another tested path planning algorithm was the Ant Colony Optimization (ACO). Both variants of the ACO algorithm, ACS and Min-Max AS, are applied to the RPAS path planning problem. The necessary elements are:

- Graph Construction: the graph is constructed as a weighted tri-dimensional grid. Each node represents the RPAS position and orientation in a Cartesian coordinate system (x,y,z,α,ψ). The spacing between the nodes is proportional to the distance between points.

- Constraints: depending on the type of platform being considered different movements are allowed as defined in Sec.5.3.2.

- Pheromone trail: in this implementation, pheromones will be deposited in each node, representing the desirability of visiting one node after the other.

- Heuristic information: defined as the inverse of the distance between each node and the target and, additionally, as the inverse of the energy expenditure between nodes, as

$$\eta_{ij} = \frac{1}{d_{ij}} \frac{1}{E_{ij}}, \qquad (29)$$

where d_{ij} represents the Euclidean distance given by Eq.(23) and E_{ij} represents the energy spend in the transition between nodes, given by Eq.(24).

To test the performance of the proposed algorithms two examples are considered: first a minimum distance path is planned in a tri-dimensional environment. In the second example a simple two-dimensional environment is used to test the planning of energy efficient paths in the presence of a wind field. The results presented consider a fixed-wing platform with 10kg of mass, wing area of 1m2 and drag coefficient of 0.5, flying at 12m/s at sea level.

Minimum distance paths

In this first example the objective is to plan a minimum distance path between two points over a 3D terrain. The map characteristics are given in Tab.6.

Table 6. Map characteristics [Alves,2016].

Map size	Start	Goal	$\Delta x = \Delta y$	Δz	D_{safety}
93x70x50	[11,88,200]	[66,53,200]	150	50	150

For the A* algorithm the cost function used is $f(n)=g(n)+h(n)$, where both $g(n)$ and $h(n)$ are Euclidean distances. In the ACO algorithm, the heuristic information is given as $\eta_{ij}=1/d_{ij}$ and the cost of the ants paths is calculated as the travelled distance between nodes. The algorithms parameters are given in Tab.7.

Table 7. ACO parameters[Alves,2016].

α	β	m	$q0$	τ	ρ	ξ	$iter$	τ_{min}	τ_{max}
1	2	10	0.4	10	0.3	0.9	500	0.01	10

The results are presented in Tab.8.

Table 8. Minimum distance paths without wind [Alves,2016].

Algorithm	Distance [m]	CPU time [s]
A*	1.0275e4	0.4609
ACS	3.9445e4	149.4950
Min-Max AS	3.8818e4	101.6099

The planned paths are shown in Fig. 16 to 18.

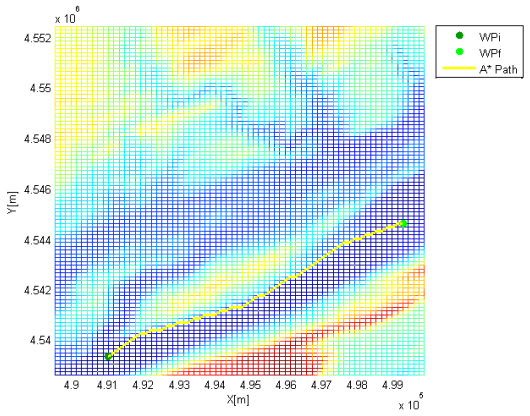

Figure 16. Minimum distance A* paths (*x-y plane*) [Alves,2016]).

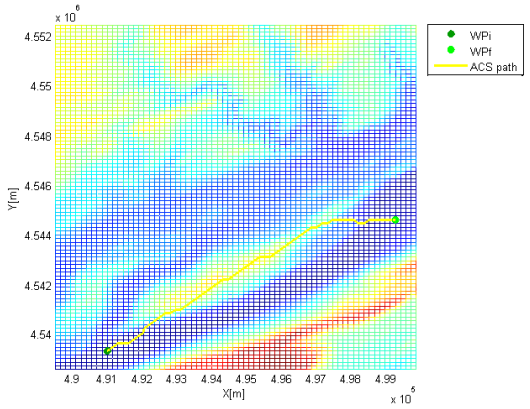

Figure 17. Minimum distance ACS paths (*x-y plane*) [Alves,2016]).

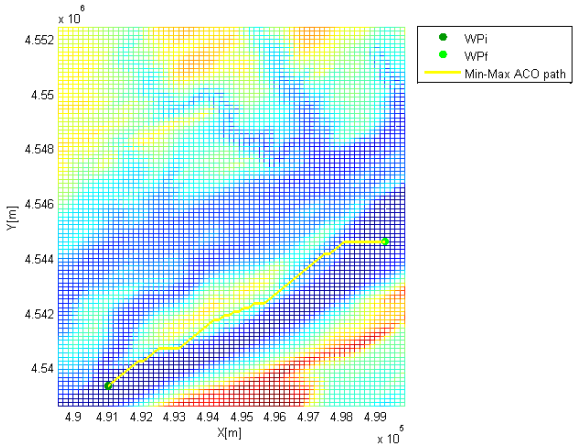

Figure 18. Minimum distance Min-Max AS paths (*x-y plane*) [Alves,2016]).

Minimum energy paths

The A* cost function is defined as $f(n)=g(n)+h(n)$, where $h(n)$ is the Euclidean distance to the goal and $g(n)$ is the

accumulated energetic cost of transitions between nodes. For the ACO, the heuristic function is given by Eq.(13). The graph characteristics for this test are presented in Tab.9. The algorithms parameters are given in Tab.10.

Table 9. Map characteristics [Alves,2016].

Map size	Start	Goal	$\Delta x = \Delta y$	D_{safety}
20x20	[60,450]	[450,60]	30	150

Table 10. ACO parameters [Alves,2016].

α	β	m	$q0$	τ	ρ	ξ	$iter$	τ_{min}	τ_{max}
1	2	10	0.4	10	0.3	0.9	1000	0.01	10

The results are given in Tab.11. and Tab.12, for with wind and without wind conditions, respectively.

Table 11. Minimum energy paths without wind [Alves,2016].

Algorithm	Energy [J]	CPU time [s]
A*	2.0467e4	0.1455
ACS	2.3322e4	137.7393
Min-Max AS	2.2140e4	110.2066

Table 12. Minimum energy paths with wind [Alves,2016].

Algorithm	Energy [J]	CPU time [s]
A*	3.7305e4	0.4609
ACS	3.9445e4	139.4950
Min-Max AS	3.8818e4	101.6099

The planned paths are shown in Figures 19 to 21, with indication of the RPAS departure heading.

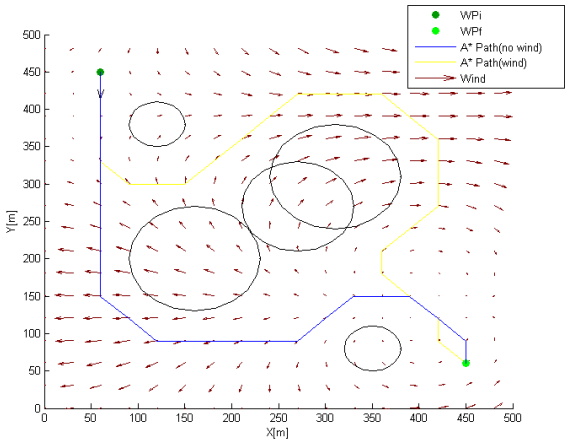

Figure 19. Minimum energy A* path [Alves,2016]).

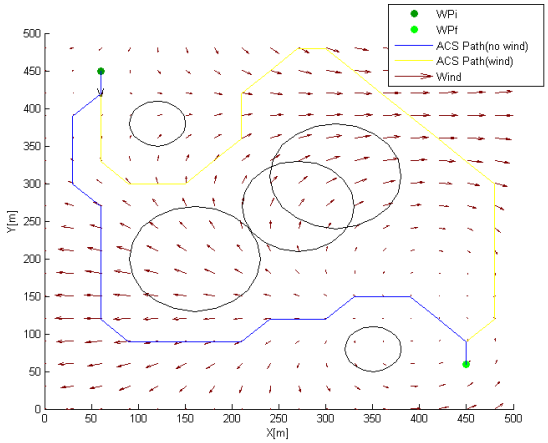

Figure 20. Minimum energy ACS path [Alves,2016]).

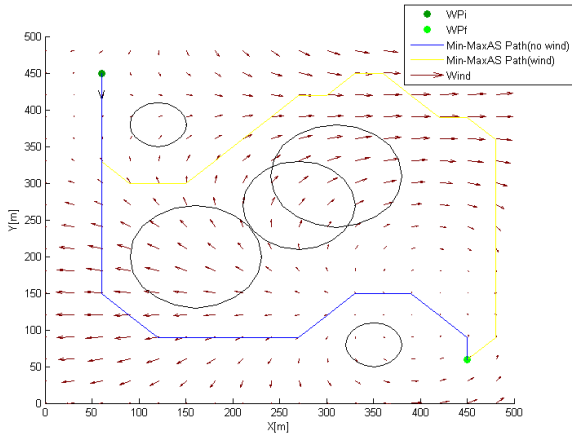

Figure 21. Minimum energy Min-Max AS path [Alves,2016]).

From the obtained results it can be concluded that the A* algorithm outperforms ACO. The drawbacks of ACO are its slow convergence and the randomness of the search does not guarantee that the optimal solution is found. On the other hand A* is complete, meaning that if a solution exists it will always find one and if used with a consistent heuristic it is guaranteed that the found path is optimal. Between the two ACO algorithms tested the Min-Max AS has shown better results in terms of computation time and path cost.

6 FINAL REMARKS

While this project is still in an early stage of development, progress has been made in every of the three safety subsystems identified. It is

expected that by the end of the project, the goals identified in Sec.1 will be successfully achieved.

ACKNOWLEDGEMENTS

This work was supported by FCT (Foundation for Science and Technology) through IDMEC (Institute of Mechanical Engineering), under LAETA, project Pest-OE/EME/LA0022. The work presented is sponsored by LAETA to leverage the multi-disciplinary competences among its several research centers, particularly in the area of Aeronautics.

This project includes the important collaboration of master students, in particular, Juliana Alves, Tiago Baião and Luís Parada.

REFERENCES

Alves, J. Path planning and collision avoidance algorithms for small RPAS, MSc Thesis, Instituto Superior Técnico, Portugal, Nov. 2016.

Bai, H., Hsu, D., Kochenderfer, M., Lee, W.S. Unmanned aircraft collision avoidance using continuous-state POMDPs, Proceedings of Robotics: Science and Systems, Los Angeles, CA, USA, Jun. 2011.

Baião, T. Energy management in RPAS, MSc Thesis, Instituto Superior Técnico, Portugal, Nov. 2016.

Başoğlu, M.E., Çakır, B. Comparisons of MPPT performances of isolated and non-isolated DC–DC converters by using a new approach. *Renewable and Sustainable Energy Reviews.* 60:1100-1113, 2016.

Cândido, L. Design of a long range solar UAV, MSc Thesis, Universidade da Beira Interior, Portugal, Oct. 2014.

Cox, T.H, Nagy, C.J., Skoog, M.A., Somers, I.A., Warner, R.. Civil UAV capacity assessement, Technical Report, NASA Dresden, 2004.

Daniel, K., Nash, A., Koenig, S., Felner, A. Theta: any-angle path planning on grids. *Journal of Artificial Intelligence Research*, 39:533-579, 2010.

Dijkstra, E.W. A note on two problems in connexion with graphs. *Numerische Mathematik.* 1(1):269-271, 1959.

Duchon, F., Babinec, A., Kajan, M. , Beno, P. , Florek, M., Fico, T., Jurisica, L. Path planning with modified A* algorithm for a mobile robot. *Procedia Engineering*, 96:59-69, 2014.

Ferreira, M. Hybrid Propulsion of a long endurance electric UAV, MSc Thesis, Instituto Superior Técnico, Portugal, Nov. 2014.

Gao, X.-Z., Hou, Z.-X., Guo, Z., Liu, J.-X, Chen, X.-Q. Energy management strategy for solar-powered high-altitude long-endurance aircraft. *Energy Conversion and Management.* 70:20-30, 2013.

Gao, X.-Z., Hou, Z.-X., Guo, Z., Chen, X.-Q. Reviews of methods to extract and store energy for solar-powered aircraft. *Renewable and Sustainable Energy Reviews*, 44:96–108, 2015.

Grøtli, E.I., Johansen, T.A. Path planning for UAVs under communication constraints using SPLAT! and MILP. *Journal of Intelligent & Robotic Systems*, 65(1):265-282, 2012.

Hwangbo, M., Kuffner, J., Kanade, T. Efficient two-phase 3D motion planning for small fixed-wing UAVs, Proceeding of IEEE International Conference on Robotics and Automation, Roma, Italy, Abr. 2007.

Karp, A. FAA Nightmare: A million Christmas drones, Aviation Daily, Sep 28, 2015.

Karunarathne, L., Economou, J.T., Knowles, K. Power and energy management system for fuel cell unmanned aerial vehicle. *ASME Part G Journal of Aerospace Engineering.* 226(4):437-454, 2012.

Kothari, M., Postlethwaite, I. A probabilistically robust path planning algorithm for UAVs using rapidly-exploring random trees. *Journal of Intelligent & Robotic Systems*, 71(2):231-253, 2013.

ICAO. Sense and avoid for unmanned aircraft systems. FAA sponsored workshop, 2014.

Liao, T. RPAS collision avoidance using A* algorithm, MSc Thesis, Auburn University, USA, 2012.

Lihua, Z., Xianghong, C., Fuh-Gwo, Y. A 3D collision avoidance strategy for UAV with physical constraints. Measurement, 77:40-49, 2016.

Filippis, L., Guglieri, G., Quagliotti, F. Path planning strategies for UAVS in 3D environments. *Journal of Intelligent and Robotic Systems*. 65(1):247-264, 2012.

Lin, Y., Saripalli, S. Sense and avoid for unmanned aerial vehicles using ADS-B, Proceedings of the IEEE International Conference on Robotics and Automation, Seattle, WA, USA, May 2015.

Luo, G.C., Yu, J.Q., Mei, Y.S., Zhang, S.Y. UAV path planning in mixed-obstacle environment via artificial potential field method improved by additional control force. *Asian Journal of Control*, 17(5):1600-1610, 2014.

Luongo, S. An optimal 3D analytical solution for collision avoidance between aircraft, Proceedings of IEEE Aerospace Conference, Big Sky, MT, USA, Mar, 2009.

Ma, G., Duan, H., Liu, S. Improved ant colony algorithm for global optimal trajectory planning of UAV under complex environment. *International Journal of Computer Science and Applications*. 4:57-68, 2007.

Marta, A.C., Gamboa, P.. Long endurance electric UAV, Proceedings of the ICAS 2014 Conference, St. Petersburg, Russia, Sep, 2014.

Miller, P. Design of a remote person view system for a long range UAV, MSc Thesis, Instituto Superior Técnico, Portugal, Jun. 2015.

NREL PV Research.. Best Research-Cell Efficiencies,.NREL, http://www.nrel.gov/pv/,2012.

Parada, L., Design of a long endurance solar UAV. MSc Thesis, Instituto Superior Técnico, Portugal, Oct. 2016.

Richards, A., How, J.P. Aircraft trajectory planning with collision avoidance using mixed integer linear programming. *Journal of Intelligent & Robotic Systems*. 65: 247-264, 2012.

Ruchti, J. RPAS Collision avoidance using artificial potential fields. *Journal of Aerospace Information Systems*, 11(3):140-144, 2014.

Saaty, T. The Analytic Hierarchy Process: Planning, Priority Setting, Resource Allocation. McGraw-Hil, 1980.

Silva, N. Parametric Design, aerodynamic analysis and optimization of a solar UAV, MSc Thesis, Instituto Superior Técnico, Portugal, Jun. 2014.

Teal Group. World Unmanned Aerial Vehicle Systems, Market Profile and Forecast 2014.

Temizer, S. Collision avoidance for unmanned aircraft using Markov decision orocesses. AIAA Guidance, Navigation and Control Conference, Aug. 2010.

Tremblay, O., Dessaint, L.-A., Dekkiche, A.-I. A generic battery model for the dynamic simulation of hybrid electric vehicles. IEEE Vehicle Power and Propulsion Conference, 2007.

Yu, X., Zhang, Y. Sense and avoid technologies with applications to unmanned aircraft systems: review and prospects. *Progress in Aerospace Sciences*, 74:152-166, 2015.